



**HAL**  
open science

## Optimization of Solid Lipid Nanoparticle Formulation for Cosmetic Application Using Design of Experiments, PART II: Physical Characterization and In Vitro Skin Permeation for Sesamol Skin Delivery

Margot Cassayre, Auriane Oline, Caroline Orneto, Emmanuel Wafo, Lydia Abou, Alexandre Altié, Magalie Claeys-Bruno, Christophe Sauzet, Philippe Piccerelle

### ► To cite this version:

Margot Cassayre, Auriane Oline, Caroline Orneto, Emmanuel Wafo, Lydia Abou, et al.. Optimization of Solid Lipid Nanoparticle Formulation for Cosmetic Application Using Design of Experiments, PART II: Physical Characterization and In Vitro Skin Permeation for Sesamol Skin Delivery. *Cosmetics*, 2024, 11 (4), pp.120. 10.3390/cosmetics11040120 . hal-04734943

**HAL Id: hal-04734943**

**<https://amu.hal.science/hal-04734943v1>**

Submitted on 14 Oct 2024

**HAL** is a multi-disciplinary open access archive for the deposit and dissemination of scientific research documents, whether they are published or not. The documents may come from teaching and research institutions in France or abroad, or from public or private research centers.






L'archive ouverte pluridisciplinaire **HAL**, est destinée au dépôt et à la diffusion de documents scientifiques de niveau recherche, publiés ou non, émanant des établissements d'enseignement et de recherche français ou étrangers, des laboratoires publics ou privés.



Distributed under a Creative Commons Attribution 4.0 International License

## Article

# Optimization of Solid Lipid Nanoparticle Formulation for Cosmetic Application Using Design of Experiments, PART II: Physical Characterization and In Vitro Skin Permeation for Sesamol Skin Delivery

Margot Cassayre <sup>1,\*</sup>, Auriane Oline <sup>2</sup>, Caroline Orneto <sup>1</sup>, Emmanuel Wafo <sup>3</sup>, Lydia Abou <sup>4</sup>, Alexandre Altié <sup>5</sup>, Magalie Claeys-Bruno <sup>1</sup>, Christophe Sauzet <sup>1,\*</sup> and Philippe Piccerelle <sup>1,\*</sup>

<sup>1</sup> CNRS, IRD, IMBE, Avignon Université, Aix-Marseille University, 13385 Marseille, France; caroline.orneto@univ-amu.fr (C.O.); m.claeys-bruno@univ-amu.fr (M.C.-B.)

<sup>2</sup> Faculty of Pharmacy, Service of Pharmacy Galenic, Industrial Pharmacotechny, Biopharmacy and Cosmetic Aix Marseille University, 13385 Marseille, France; auriane.oline@orange.fr

<sup>3</sup> INSERM, SSA, MCT, Aix-Marseille University, 13385 Marseille, France; emmanuel.wafo@univ-amu.fr

<sup>4</sup> INRAE, INSERM, C2VN, Aix-Marseille University, 13385 Marseille, France; lydia.abou@univ-amu.fr

<sup>5</sup> CNRS, CINAM, Aix-Marseille University, 13009 Marseille, France; alexandre.altie@cnrs.fr

\* Correspondence: cassayre.margot@gmail.com (M.C.); christophe.sauzet@univ-amu.fr (C.S.); philippe.piccerelle@univ-amu.fr (P.P.); Tel.: +33-6-77-44-56-95 (M.C.)

**Abstract:** Our research focuses on evaluating the preliminary stability of solid lipid nanoparticles (SLNs) in order to identify an optimal formulation for studying the skin penetration of SLNs loaded with sesamol, with a view to developing potential cosmetic applications. For this study, SLNs were prepared with varying lipid and surfactant compositions and produced through homogenization and ultrasonication. The particle size (PS), polydispersity index (PDI), zeta potential (ZP), and encapsulation efficiency (EE) were analyzed for the different formulations. We identified OP2Se as the optimal formulation for skin penetration assessment due to its stable PS, PDI, ZP, and EE over time, with a Turbiscan Stability Index (TSI) below 1 after a month, indicating favorable stability conditions. The in vitro skin permeation study compared sesamol-loaded SLNs with a control sesamol hydrogel, revealing controlled release characteristics ideal for localized skin effects without significant bloodstream penetration, attributed to the SLNs' 200 nm particle size. Further exploration could enhance skin retention and targeting, potentially extending penetration studies and reducing particle size to improve accumulation in hair follicles. Exploring SLN applications beyond sesamol, such as incorporating mineral filters for suncare, offers promising avenues, underscoring SLNs' versatility in cosmetic formulations and skincare applications.

**Keywords:** solid lipid nanoparticle (SLN); formulation; physical characterization; stability; sesamol; skin permeation



**Citation:** Cassayre, M.; Oline, A.; Orneto, C.; Wafo, E.; Abou, L.; Altié, A.; Claeys-Bruno, M.; Sauzet, C.; Piccerelle, P. Optimization of Solid Lipid Nanoparticle Formulation for Cosmetic Application Using Design of Experiments, PART II: Physical Characterization and In Vitro Skin Permeation for Sesamol Skin Delivery. *Cosmetics* **2024**, *11*, 120. <https://doi.org/10.3390/cosmetics11040120>

Academic Editor: Lucia Montenegro

Received: 22 April 2024

Revised: 17 June 2024

Accepted: 24 June 2024

Published: 15 July 2024



**Copyright:** © 2024 by the authors. Licensee MDPI, Basel, Switzerland. This article is an open access article distributed under the terms and conditions of the Creative Commons Attribution (CC BY) license (<https://creativecommons.org/licenses/by/4.0/>).

## 1. Introduction

In recent years, solid lipid nanoparticles (SLNs) have garnered significant attention as promising drug delivery carriers due to their unique properties, including enhanced stability, controlled release, and improved bioavailability [1,2]. These nanoparticles offer a potential solution for overcoming challenges associated with conventional drug delivery systems and facilitating targeted delivery to specific tissues, such as the skin [3]. Indeed, their small size and high surface area allow them to penetrate and accumulate in the skin layers more effectively compared to larger particles or conventional formulations [4]. Moreover, SLNs are composed of lipids such as fatty acids, triglycerides, and waxes which enhance their biocompatibility and interaction with the lipophilic stratum corneum layer of the skin, improving skin permeation [5].

Furthermore, SLNs have emerged as a promising and innovative delivery system in the field of cosmetics. SLNs offer several distinct advantages that make them an attractive option for enhancing the performance and efficacy of cosmetic products [6]. These advantages include improved stability, controlled release of active ingredients, enhanced skin penetration, and the ability to encapsulate and protect both hydrophilic and hydrophobic compounds [7]. As reported by Müller et al. [7], the lipid matrix in SLNs provides a protective environment for encapsulated ingredients, reducing degradation and improving shelf life. Furthermore, SLNs' nanoscale size promotes better skin hydration and the targeted delivery of bioactive compounds [8]. Overall, the incorporation of SLNs in cosmetic formulations holds great potential for advancing the efficacy and functionality of modern cosmetic products.

The formulation of SLNs is a complex process and is influenced by multiple factors, such as lipid type, surfactant composition, and processing parameters [9]. To achieve efficient drug delivery and good stability, it is essential to adapt the SLN formulation to the specific drug and targeted tissue [10].

In prior research, we presented the results of a novel approach combining mixture and quantitative variables to optimize an SLN composition for cosmetics application. This comprehensive investigation explored the influential factors (percentage of polysorbate 80; time of ultrasound; and proportion of carnauba wax, glyceryl behenate, and glyceryl distearate) and their interactions. These experimentations led us to the identification of an optimized SLN formulation, with a particle size (PS) of  $176.3 \pm 2.78$  nm, a polydispersity index (PDI) of  $0.268 \pm 0.02$ , and a zeta potential (ZP) of  $-35.5 \pm 0.36$  mV. Interestingly, the experimental design revealed that achieving the desired results could accommodate only minor variations in emulsifier composition, while substantial flexibility was observed in lipid composition. This previous study shed light on the critical role of lipid and surfactant components, as well as on the process parameter to obtain SLNs, offering valuable insights for the development of efficient cosmetic delivery systems for sesamol [11].

Sesamol, a natural phenolic compound derived from sesame oil, has garnered significant attention in the field of cosmetics due to its various properties. Its potent antioxidant activity, as shown by studies such as those conducted by Srisayam et al. [12] and Geetha et al. [13], makes sesamol an ideal candidate for combatting oxidative stress-induced skin damage. Moreover, sesamol has demonstrated anti-inflammatory effects, as highlighted by Prado et al. [14], which offer potential benefits in soothing and calming inflammatory skin. The compound's ability to inhibit melanin production, as indicated by Wu et al. [15] and Mahendra Kumar et al. [16], also paves the way for addressing hyperpigmentation concerns. These promising characteristics make sesamol a promising ingredient for innovative topical formulations aimed at promoting skin health, enhancing its appearance, and reducing hyperpigmentation disorders.

In our study, we chose sesamol for its depigmenting ability. Additionally, its anti-inflammatory and antioxidant actions are advantageous as these mechanisms also play a role in pigmentation processes, making sesamol a multifaceted molecule of interest in our research. Therefore, we chose to incorporate sesamol into our SLNs to enhance its penetration (because of the deep location of melanocytes in the basal layer of the epidermis), aiming for improved efficacy.

This work aims to provide insights into the potential of sesamol-loaded SLNs as an effective skin delivery system compared to conventional cosmetic vehicles such as hydrogels. Sesamol-loaded SLNs were selected among four formulations obtained from a design of experiments (DOE) analysis using desirability tools. The choice of sesamol-loaded SLNs for the *in vitro* comparison test (skin permeation) was based on the evaluation of physicochemical properties, preliminary stability, and encapsulation efficiency.

## 2. Materials and Methods

### 2.1. Materials

Carnauba wax (T-1) provided by IMCD France (Lyon, France) and glyceryl distearate (Precirol ATO) and glyceryl behenate (Compritol 888 CG pellets) obtained from Gattefossé (Saint-Priest, France) were used as the lipid materials. Polysorbate 80 (Tween<sup>®</sup> 80) and sorbitan oleate (Span<sup>®</sup> 80) were kindly gifted by Croda (Montigny-le-Bretonneux, France) and were used as the emulsifiers in the formulation. Disodium phosphate anhydrous and citric acid were purchased from Cooper (Melun, France) and used for the buffer present in the hydrogel. Glycerin was kindly gifted by Ies Labo (Oraison, France), as was propanediol from IMCD France (Lyon, France), and both were used as humectants in the hydrogel. The gelling agent, xanthan gum, was obtained from AMI ingredient (Tauxigny-Saint-Bauld, France). Lastly, phenethyl alcohol was used as a preservative and was kindly gifted by Evonik (Ham, France).

Sesamol, methanol, and DMSO were purchased from Sigma Aldrich (Saint Quentin Fallavier, France).

### 2.2. Variation Domain Determination of the Formulations

We based the SLN preparation on the mathematical predictions of an optimized formulation (OP4) [11] taken from a previous design of experiments (DOE) conducted for the obtention of SLNs containing no active ingredient. This formulation coincided with the maximum desirability obtainable with our variables (Table 1).

**Table 1.** Studied factors with their domains of variation: for X1 variation domain expressed as a percentage of surfactant and co-surfactant amount representing 10% of the final composition and for X3 to X5 variation domain expressed from 0 to 1 representing 5% of the final formulation.

Variable	Factors	Nature of the Factor	Variation Domains
X <sub>1</sub>	Percentage of polysorbate 80 (P80) in P80/SO couple	Quantitative variable	0 to 100%
X <sub>2</sub>	US time	Quantitative variable	1 to 10 min
X <sub>3</sub>	Proportion of carnauba wax (CW)	Mixture variable	0 to 1
X <sub>4</sub>	Proportion of glyceryl behenate (GB)	Mixture variable	0 to 1
X <sub>5</sub>	Proportion of glyceryl distearate (GDS)	Mixture variable	0 to 1

However, in order to study the stability and the sesamol encapsulation of SLNs over time, we decided to study the range of desirability around this optimized formulation while keeping as close as possible to the responses we were expecting, i.e., a particle size as close as possible to 100 nm, a PDI as close as possible to 0, and a ZP as high as possible in absolute value and close to 40 mV (Figure 1).

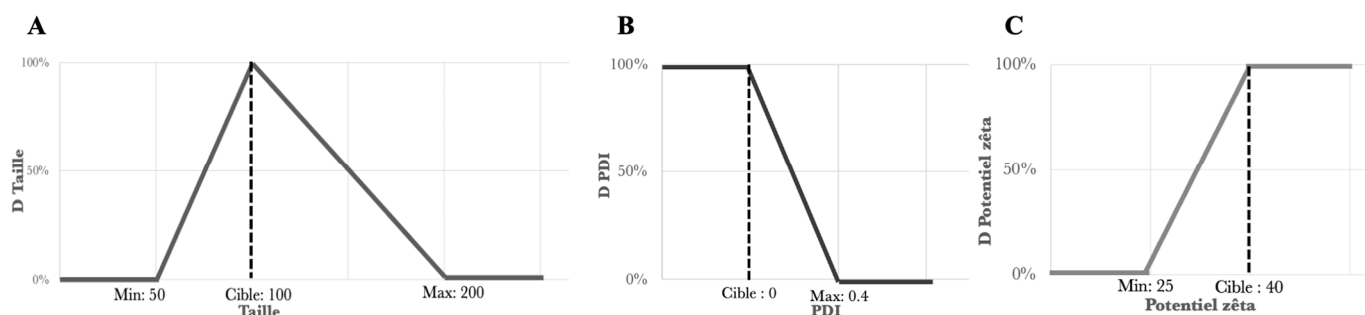


**Figure 1.** Responses for the desirability function approach. (A) Desirability for particle size (nm); (B) Desirability for PDI; (C) Desirability for zeta potential (mV).

This is why we decided to choose 3 other formulations that best matched these criteria in the DOE results. All the chosen formulations matched the target values but with different compositions. The compositions of the formulations with (OPSe) and without (OPb) sesamol are presented in Table 2.

**Table 2.** Composition of the blank (b) and sesamol-loaded (Se) optimized (OP) SLNs.

	% Water	% Carnauba Wax (CW)	% Glyceryl Behenate (GB)	% Glyceryl Distearate (GDS)	% Polysorbate 80 (P80)	% Sorbitan Oleate (SO)	% Sesamol	US Time (min)
OP1b	85	1.75	1.55	1.7	3.02	6.98	-	7
OP1Se	84.8	1.75	1.55	1.7	3.02	6.98	0.2	7
OP2b	85	3.17	1.73	0.1	3.81	6.19	-	10
OP2Se	84.8	3.17	1.73	0.1	3.81	6.19	0.2	10
OP3b	85	0.44	3.5	1.07	3.2	6.84	-	7.12
OP3Se	84.8	0.44	3.5	1.07	3.2	6.84	0.2	7.12
OP4b	85	2.93	1.1	0.97	4.09	5.91	-	7.5

### 2.3. HPLC Analysis of Sesamol

The quantification of sesamol was performed through HPLC UltiMate™ 3000 using a diode array detector (Thermo Scientific™, Dionex, France). Chromeleon HPLC software (version 6.8) was used to perform integration of the peaks. Separation was carried out in an Uptisphere® UP 5PAH column at room temperature (Interchrom-Interchim, Montluçon, France). Chromatographic separation was carried out with a mobile phase of water/acetonitrile (40:60) at 1 mL.min<sup>-1</sup>. The injection volume was 10 µL. Detection was achieved using a diode array detector (UVD340U Dionex) at wavelengths ranging from 200 to 600 nm, while the sesamol detection was performed at 290 nm. An analytical curve ( $n = 6$ ) was prepared in the range of 2.343–300 µg/mL which displayed good linearity ( $r^2 = 0.9998$ ). All the samples were measured in triplicate. HPLC analysis was performed for both encapsulation efficiency and permeation studies.

### 2.4. Preparation of Blank Optimized SLNs (OPb) and Sesamol-Loaded Optimized SLNs (OPSe)

The compositions of the blank and sesamol-loaded optimized SLNs are reported in Table 2.

The SLNs were produced using hot homogenization followed by the ultrasonication method. Briefly, the solid lipids (carnauba wax (CW), glyceryl behenate (GB), and/or glyceryl distearate (GDS)) were melted at 92 °C with sorbitan oleate (SO) as an emulsifier. The sesamol was added to the lipid phase once the latter was completely melted, and magnetic agitation continued for few minutes to ensure that the sesamol was solubilized. The aqueous phase, consisting of a dispersion of polysorbate 80 (P80) in water with magnetic agitation, was also heated at 92 °C. Once both phases were at the required temperature, the hot aqueous phase was dispersed in the melted lipidic phase using high-speed stirring with a T 25 ULTRA-TURRAX® disperser (IKA®—Werke GmbH and Co., KG, Staufen, Germany) at 10,000 rpm for 7 or 10 min at 92 °C ± 3 °C. Then, the resulting primary emulsion was sonicated with a probe sonicator (Ultrasonics™ Sonifier™, SFX550, Fisher Scientific, Illkirch, France) and cooled in an ice bath to obtain the solid nanodispersions.

### 2.5. Preparation of Sesamol Hydrogel

Given our aim to study the penetration of sesamol for cosmetic applications, we chose to compare the penetration of SLNs with that of a hydrogel, which is a common base formulation in cosmetics. Hydrogel was prepared using a cold process. First of all, a citrate phosphate buffer with a pH of 5.5 was prepared from the European pharmacopeia (Ph. Eur. 10.0; 4.1.3.4008700), for which 568.5 mL of an anhydrous disodium phosphate solution R at 28.4 g/L and 43.15 mL of a citric acid monohydrate solution at 21 g/L were mixed together. Secondly, 1 g of the preservative (phenethyl alcohol) was added to 91.49 g of the

buffer under agitation and left for 5 min to ensure solubilization. A premix of glycerin (3 g), propanediol (4 g) and xanthan gum (0.5 g) was then added to the buffer. The sesamol (0.2 g) was incorporated at the end of the process. The final macroscopic aspect of the hydrogel was completely transparent, which enabled us to ensure complete solubilization of the sesamol in addition to its water solubilization limit.

### 2.6. Analysis of Particle Size (PS) and Polydispersity Index (PDI)

In this section, we outline the methodology used for the analysis of PS and PDI in our study. The characterization of particles is crucial for understanding their physico-chemical properties and behavior in various systems. We used dynamic light scattering (DLS) to determine the PS and PDI of the samples under investigation using a Malver Zetasizer Nano ZS90 (Malvern Instruments Ltd., Worcestershire, UK). The mean particle size (z-average diameter) and PDI were obtained by averaging the measurements at an angle of 90°.

Prior to the measurement, distilled water was used to dilute all the samples in order to ensure a suitable scattering intensity. Each sample was then loaded into a disposable cuvette, and measurements were taken at a controlled temperature of  $25 \pm 2$  °C. All the experiments were carried out in triplicate.

### 2.7. Zeta Potential (ZP) Analysis

The ZP of particles is a critical parameter that influences stability, aggregation, and interactions with other entities in a dispersion. To determine the zeta potential, the device employs two measurement techniques: electrophoresis and laser Doppler to analyze the electrophoretic mobility measurements. A Malver Zetasizer Nano ZS90 (Malvern Instruments Ltd., Worcestershire, UK) at a temperature of  $25 \pm 2$  °C was used for these measurements. Prior to analysis, the samples were diluted with distilled water to achieve the optimal concentration, ensuring that the measured electrophoretic mobility was within the instrument's detection range. All the experiments were carried out in triplicate.

### 2.8. Encapsulation Efficiency (EE)

The EE of sesamol present in the SLN formulations was determined using the ultrafiltration method.

We were inspired by the method of Madureira et al. [17] with some modifications. First, 4 mL of SLNs were introduced into an Amicon Ultra-4 10 K centrifugal device (Millipore, Carrigtwohill, Ireland), with a 10 kDa molecular weight cut-off. Centrifugation was performed at 20 °C for 1 h at 4400 rpm using an Eppendorf 5702 RH centrifuge. The ultrafiltrate was then recovered and analyzed using HPLC to determine the concentration of encapsulated sesamol.

The encapsulation efficiency (EE) values were calculated according to the following formula:

$$(EE)\% = \frac{\text{Total amount of sesamol} - \text{Free amount of sesamol}}{\text{Total amount of sesamol}} \times 100$$

### 2.9. Preliminary Stability Studies

The main purpose of these studies is to determine the best SLN candidate with sesamol for skin permeation evaluation. To achieve this, a preliminary stability study was conducted over 30 days (at room temperature storage) and supplemented with Turbiscan analysis to predict long-term stability. However, a more comprehensive stability assessment of the SLNs will be necessary in subsequent studies.

#### 2.9.1. PS, PDI, ZP, and EE Stability

The physical stability of the SLNs was assessed by recording changes in PS, PDI, ZP, and EE over a period of 30 days upon storage at room temperature. An aliquot of the



sample was taken after 0, 15, and 30 days of storage, and PS, PDI, ZP, and EE were explored as described above.

### 2.9.2. Turbiscan Stability

The stability of the SLNs was also evaluated using Turbiscan<sup>®</sup> Lab (Formulation, Toulouse, France). Turbiscan<sup>®</sup> Lab has previously been reported as a reliable technology [18] for evaluating the occurrence of instability phenomena such as particle aggregation and/or migration. The SLNs were transferred immediately after preparation into a cylindrical glass cell and analyzed using static multiple light scattering (SMLS) to detect particle migration and size variation in liquid dispersions. SMLS consists in sending photons in near infrared (880 nm) wavelength by scanning the sample cell. These photons are detected by two synchronous detectors: transmission (0°) from the light source for the transparent sample and backscattering (135°) for the opaque sample. The backscattering (BS) is directly dependent on the particle mean diameter and the particle concentration. [19]

The sample in the cell was scanned for 24 h (at D-0 and D-30) every 15 min at 25 °C, and we looked at the variation in the percentage of backscattering scan and the TSI (Turbiscan Stability Index) during the experiment to measure the SLN stability.

The calculation of the TSI (Turbiscan Stability Index) is based on the comparison of each scan with the previous, according to the following formula:

$$\text{TSI} = \sum_i \frac{\sum_h [\text{scan}_i(h) - \text{scan}_{i-1}(h)]}{H}$$

Each scan at a given height is subtracted from the previous scan at the same height; the whole is summed and divided by the total height of the sample. The result is therefore independent of the amount of product present in the cell.

### 2.10. Scanning Electron Microscopy (SEM) Analysis

The morphology of the nanoparticles was evaluated using the scanning electron microscopy (SEM) technique. A JEOL JSM-7900F microscope (Tokyo, Japan) was used. Briefly, a small amount of diluted SLNs were placed on a silicon wafer support attached to a stub and placed under vacuum for several minutes to dry the sample using a turbomolecular pump. SEM was operated in standard mode (SEM) at 5 kV (WD = 11 mm using chamber secondary electron detector) and using 2 kV decelerating GB (gentle beam) mode for a final accelerating voltage of 1 kV (WD = 4 mm using in-lens secondary electron detector), which is a specific mode to analyze isolated materials without carbon deposition. All analyses were performed at room temperature (20 °C). Digital images were acquired using already owned JEOL SEM-PC software (version 3.0).

### 2.11. Differential Scanning Calorimetry (DSC) Analysis

DSC was performed to characterize the thermal behavior of the OP2 SLNs by using a DSC 25 instrument (TA instrument, New Castle, DE, USA). The nanoparticles were lyophilized using an Alpha 1–4 LCS (Christ, Fisher Scientific, France). Then, 50 mL of SLNs were placed in a 100 mL glass bottle. The entire bottle containing the nanoparticle preparations was placed at −25 °C overnight. To be freeze-dried, the samples underwent an initial primary desiccation phase with a condenser temperature of −55 °C and a vacuum set at 1.030 mbar, followed by a secondary desiccation phase lasting approximately 6 h with a plateau temperature set to 30 °C and a maximum vacuum of 0.0054 mbar.

Briefly, 5–7 mg of freeze-dried SLNs were placed in a hermetic aluminum pan. The system was calibrated using an indium standard, and the sample was run against a hermetic empty reference pan. The analyses were performed from 20 °C to 100 °C at a heating rate of 10 °C min<sup>−1</sup> by flushing with nitrogen at a rate of 80 mL/min to obtain an inert gas atmosphere in the DSC cell. TRIOS software (version 5.1) was used to obtain the DSC thermograms.

The OP2b and OP2Se SLNs, as well as all the raw materials used in the formulations, were tested.

### 2.12. *In Vitro* Skin Permeation Study

The penetration studies were carried out on non-dermatomed human skin discs taken from breast with a diameter of 18 mm.

The skin discs came from Caucasian and African donors aged between 27 and 51 years old and were purchased from the Alphenyx company (Marseille, France). The skin discs were stored at  $-20\text{ }^{\circ}\text{C}$  while awaiting the experiment.

Permeation studies using non-dermatomed human breast skin were performed on Franz diffusion cells with an effective diffusion area of  $1\text{ cm}^2$  and a receiving chamber volume of approximately 8 mL. The skin was mounted on Franz cells with the stratum corneum side up, and the temperature to be reached was  $32\text{ }^{\circ}\text{C}$ . Transepidermal water loss was measured using a Tewameter TM 300 (Monaderm, Monaco) before starting the experiment to ensure skin integrity. The receptor compartment contained PBS (pH 7.4) at  $37\text{ }^{\circ}\text{C}$ . A volume of 500  $\mu\text{L}$  of the formulations (gel or SLN) was applied to the skin surface. At various times over an 8-hour period, 200  $\mu\text{L}$  of the receptor compartment was removed and replaced with the same amount of fresh PBS. After the last sample collection, the cells were dismantled and the skin of each cell was wiped with cotton buds to remove any remaining formulation. The cotton buds were mixed with 2 mL of methanol or DMSO overnight to extract the active ingredients and then filtered using a  $0.45\text{ }\mu\text{m}$  filter. Methanol was used for the extraction of sesamol from the hydrogel and DMSO was used to extract sesamol from the SLNs.

To measure the amount of sesamol that was retained in the stratum corneum, tape stripping was then performed [20,21]. D-Squame tape discs (D-Squame tapes, Monaderm, Monaco) were applied to the exposed skin surface 21 times for approximately 5 s using an applicator ( $225\text{ g/cm}^2$ ) before being carefully removed. The first tape was set aside with 1.4 mL of methanol or DMSO, and the 20 remaining tapes were placed in separate falcons and stored overnight with 2 mL of methanol or DMSO to extract the sesamol removed from the stratum corneum (SC) by the tapes. The rest of the skin was also put in a flacon with 2 mL of methanol or DMSO and stored overnight to extract the sesamol. All the samples were then vortexed for 2 min and exposed to 1 cycle of ultrasonic bath for 30 min before being filtered with a  $0.45\text{ }\mu\text{m}$  filter and analyzed by HPLC.

### 2.13. *Data Analysis*

In this study, all experiments were conducted in triplicate to ensure the accuracy and reliability of the results. The measured differences were analyzed using Student's *t*-test, with the significance level set at 0.05. During stability testing, we initially assessed if there was a difference between D-0 and D-30. If a difference was observed, it was considered significant; however, if no difference was detected, we further examined if there were any temporal variations over the storage period.

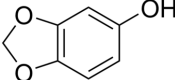
## 3. Results and Discussion

### 3.1. *Chemical Structure and Physicochemical Properties of Sesamol*

In addition to its biological properties, the choice of sesamol as the agent studied for skin penetration is supported by its chemical structure and physicochemical properties. Sesamol, with a molecular weight of  $138.12\text{ g/mol}$ , is relatively small, which facilitates its permeation through the skin. Its partial solubility in water and a moderate Log P value of 1.29 indicate a balanced hydrophilic–lipophilic nature, which is advantageous for skin absorption (Table 3).



**Table 3.** Chemical structure and physicochemical properties of sesamol [15].

Cas Number	Chemical Structure	Molecular Weight	Water Solubility	Log P	Melting Point	Protection Condition
533-31-3		138.12 g/mol	Partially	1.29	62–65 °C	Light

### 3.2. Preparation of Blank Optimized SLNs (OPb) and Sesamol-Loaded Optimized SLNs (OPSe)

In order to select suitable compositions for sesamol-loaded SLNs, a multiplicative model of experimental design was created by crossing a mixture design with quantitative design [11]. For the OPSe, sesamol powder was well dispersed in the waxy phase under magnetic stirring. A rapid visual check of the sesamol solubilization was performed at the end, and no sesamol precipitation was observed. We found that the lipid and surfactant composition and the ultrasound time had an impact on the PS, PDI, and ZP of both nanoparticles. However, each constituent of the formulation impacts the results in a different way. This is why we decided to select four optimized formulations with the best desirability and different lipid compositions and ultrasound times to observe their stability over a one-month period. Indeed, the surfactant composition was kept between 30 and 40% for all the formulations according to the results obtained from the experimental design conducted in the first article [11]. The ultrasonication method for homogenization of the SLNs was selected because it is a reproducible and efficient method to produce SLNs.

### 3.3. Analysis of Particle Size (PS) and Polydispersity Index (PDI)

The particle size (PS) and polydispersity index (PDI) of the formulations are given in Table 4.

**Table 4.** Mean values  $\pm$  SD of the physical properties of particle size (PS), polydispersity index (PDI), and zeta potential (ZP) of the produced nanoparticles on D-0.

	OP1b	OP1Se	OP2b	OP2Se	OP3b	OP3Se	OP4b	OP4Se
PS (nm)	227.37 $\pm$ 2.85	239.47 $\pm$ 13.49	182.77 * $\pm$ 6.07	213.5 * $\pm$ 7.07	215.63 $\pm$ 2.12	225.43 $\pm$ 6.79	176.3 * $\pm$ 2.78	194.27 * $\pm$ 3.86
PDI	0.27 $\pm$ 0.02	0.293 $\pm$ 0.01	0.274 $\pm$ 0.04	0.28 $\pm$ 0.01	0.265 $\pm$ 0.02	0.295 $\pm$ 0.05	0.268 $\pm$ 0.02	0.296 $\pm$ 0.02
ZP (mV)	−29.93 * $\pm$ 1.83	−35.82 * $\pm$ 2.57	−31.67 $\pm$ 0.50	−36.42 $\pm$ 2.36	−32.7* $\pm$ 0.70	−39.5 * $\pm$ 1.37	−35.5 $\pm$ 0.36	−36.14 $\pm$ 0.28

\* The differences between the means of OPb and OPSe are statistically significant ( $p < 0.05$ ) ( $n = 3$ ).

The PS on D-0 of the optimized SLNs varied from  $176.3 \pm 2.78$  to  $239.47 \pm 13.49$  nm over the eight experiments depending on the formulation composition. For OP2 and OP4, there was a significant size difference between SLNs that contained sesamol and their counterparts that did not. This could be explained by the fact that sesamol is inside the lipidic core, causing an increase in particle size [22]. On the other hand, for OP1 and OP3, no significant size difference was observed. Indeed, the %EE was smaller than that of OP2 and OP4 (Figure 2), so there was less sesamol inside the lipidic core, which may explain the absence of a difference in size.

PDI values between 0.1 and 0.3 are considered to indicate narrow dispersion, and broad dispersions are reflected by PDI values  $> 0.3$  [23]. Hence, all the formulations can be described as narrow dispersions, because for the majority of the experiments, the PDIs were between 0.25 and 0.3. These PDI values indicate good homogeneity in terms of SLN size. Moreover, there was no significant difference regarding the PDI with the addition of sesamol in the SLNs.

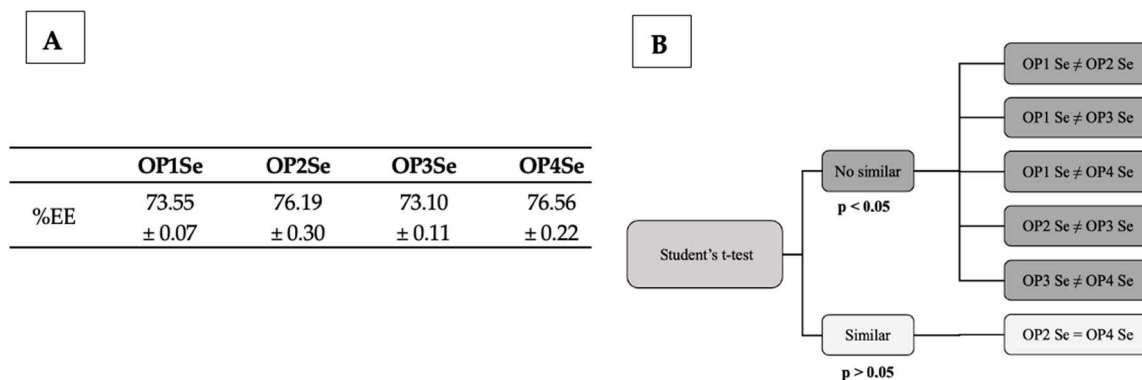


**Figure 2.** (A) Mean values  $\pm$  SD of the encapsulation efficiency (EE) of the produced nanoparticles at D-0 and (B) Student's *t*-test results of the percentage of encapsulation efficiency (%EE).

### 3.4. Analysis of Zeta Potential (ZP)

The zeta potential indicates the repulsion between charged particles in a dispersion. To prevent the aggregation of suspended particles and thus ensure good physicochemical stability, it is necessary to have a relatively high absolute value of zeta potential [24]. On the other hand, in cases where the magnitude of the zeta potential approaches a low absolute value, the resultant reduction in interparticle repulsive forces leads to particle aggregation. Hence, the zeta potential serves as a valuable metric for assessing formulation stability [25]. The incorporation of sesamol into SLNs showed a significant difference regarding the zeta potentials of the nanoparticles ( $p < 0.05$ ), except for the OP4 and OP2 formulations. As we can see, the encapsulation of sesamol sometimes induces a charge increase in the electrical double layer forming at the SLN surface. Notwithstanding the contribution of sesamol in the ZP, all formulations were negatively charged (Table 4), and the zeta potential varied from  $-29.93 \pm 1.83$  mV to  $-39.5 \pm 1.37$  mV, indicating a relatively good stability of the system.

The threshold of particle agglomeration is indicated at a zeta potential range between  $-20$  mV and  $-11$  mV [26]. Here, the modification of the surfactant composition is shown to have had a significant influence on the zeta potential of the nanoparticles (OPb) [11], enhanced by the encapsulation of sesamol (OPSe), as we can see in Table 4. The ZP mainly increased due to the inclusion of a higher proportion of SO compared to P80 in all formulations [11]. The combination of these two phenomena is aimed at improving the stability of the SLNs by increasing the zeta potential.

### 3.5. Encapsulation Efficiency (EE)

The encapsulation percentage is an essential parameter to be calculated concerning SLNs. Indeed, this parameter allows for a precise evaluation of the efficiency with which the active compound—in this case, sesamol—is trapped within the SLNs. By quantifying the percentage of encapsulated sesamol, we gain insights into the formulation's ability to deliver the active ingredient to its target with precision. This information plays a decisive role in optimizing SLNs, with the aim of enhancing the bioavailability of sesamol and advancing the potential cosmetic applications of SLNs. In this context, evaluating the sesamol encapsulation percentage within SLNs becomes a crucial step in assessing the influence of lipid composition on EE.

This parameter was measured using HPLC after ultrafiltration with Amicon as described above.

After the Student *t*-test, we could see a significant difference in the %EE between each group pair, except for OP2Se and OP4Se (Figure 2). Indeed, the composition of the SLNs leads to a variation in the %EE. The group pair OP2Se/OP4Se, which presented the same behavior regarding sesamol encapsulation from the Student *t*-test, exhibited the highest percentage of EE at 76.19 and 76.56%, respectively. This could be explained by their higher amount of carnauba wax. The good affinity between the active ingredient

and the lipid mixture might result in the high percentage of sesamol encapsulation. The Student *t*-test results show that with CW proportions between 0.44% and 2.93%, the %EE was significantly different for each group and higher than 70%. Furthermore, with  $CW \geq 2.93\%$ , the %EE was similar for each group. However, all four formulations presented an acceptable percentage of encapsulation superior to 73%.

### 3.6. Preliminary Stability Studies

The physical preliminary stability of the SLNs was evaluated over a period of 30 days of storage at 25 °C.

#### 3.6.1. Particle Size (PS) and PDI Stability

Figure 3 represents the variation in PS and Figure 4 the variation in PDI over the storage period.

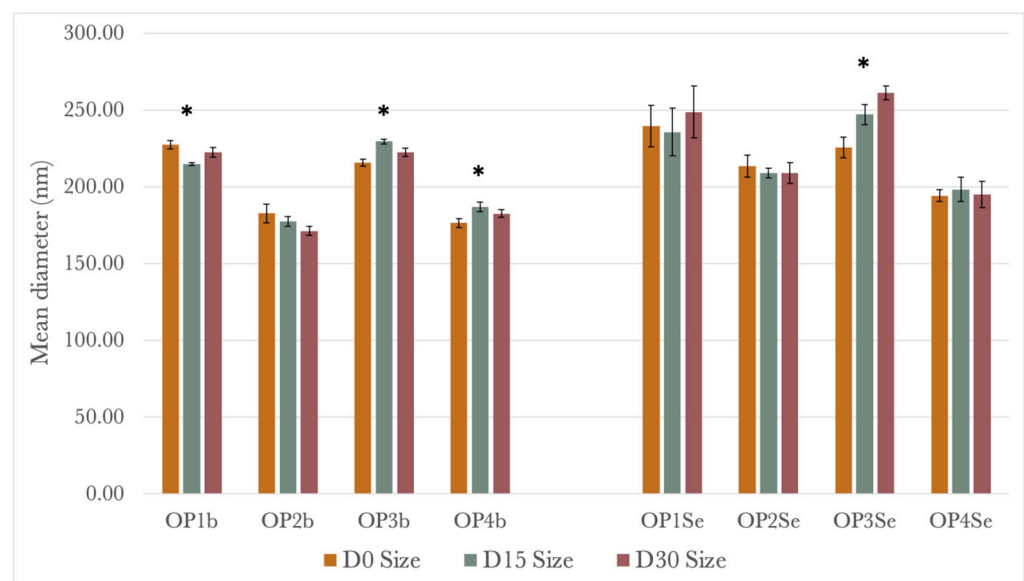


**Figure 3.** Mean PS distribution of blank (b) and sesamol (Se)-loaded optimized SLNs at different times (D-0, D-15, and D-30). \* Significant difference in PS during storage ( $p < 0.05$ ) ( $n = 3$ ).

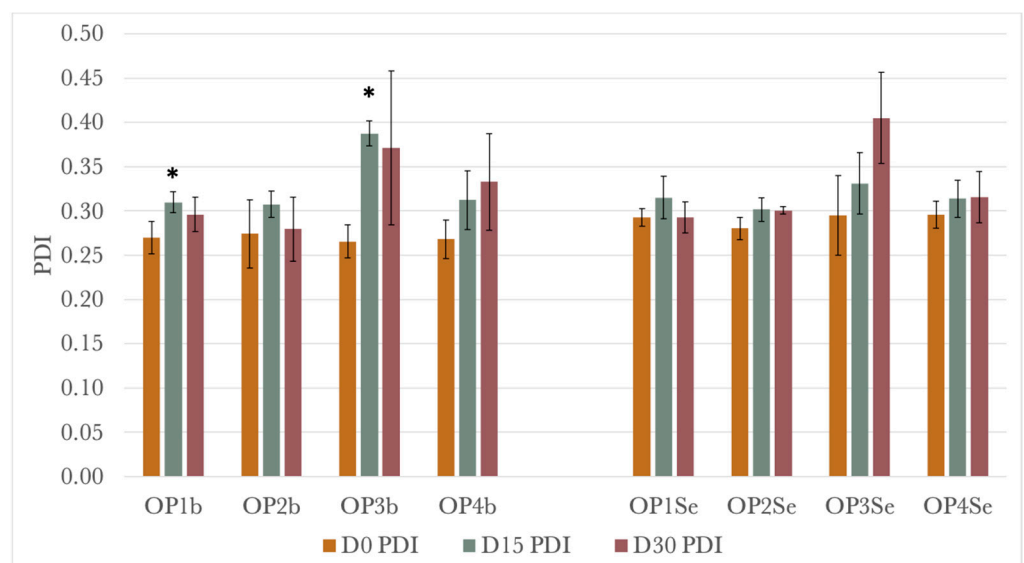


**Figure 4.** Mean PDI distribution of blank (b) and sesamol (Se)-loaded optimized SLNs at different times (D-0, D-15, and D-30). \* Significant difference in PDI during storage ( $p < 0.05$ ) ( $n = 3$ ).

As shown in Figure 3, all blank formulations showed significant PS variations, except OP2b, and most of the loaded SLNs with sesamol showed no significant PS variation during storage. As we can see, the OP3 SLNs showed a significant variation in size in both conditions, which is probably a sign of instability. In this case, sesamol probably had an influence on the size variation. This could be due to its amphiphilic properties, which allow it to be adsorbed on the SLNs' surface and thus stabilize the size variation [27].

As previously mentioned, when the PDI is below 0.3, it indicates a narrow particle size distribution. Upon examination of the different formulations, it became apparent that only OP1b and OP3b SLNs exhibited a significant variation in PDI, which probably points towards an additional indicator of instability (in addition to size variation) (Figure 4).

Sesamol encapsulation leads to stabilization of the particle size and PDI. This phenomenon was visible for OP1Se and OP3Se. In this last case, OP3Se was the only one exhibiting a PDI > 0.4 during storage without a significant variation. An increase or a variation in PDI indicates that the nanoparticle distribution is becoming progressively more dispersed, reinforcing the risk of instability (such as flocculation, Oswald ripening, and sedimentation).

### 3.6.2. Zeta Potential (ZP) Stability

An analysis of the different formulations over the 30 days of storage revealed that all formulations containing sesamol presented no significant variation in zeta potential (Figure 5). On the other hand, almost all blank SLNs (except OP4b) presented a variation in zeta potential during storage. It is possible that sesamol, as an amphiphilic molecule, could be adsorbed on the surface of SLNs and could contribute to the electrostatic stability of the particles [27]. In addition, sesamol can also help stabilize SLNs by preventing the migration of water through the lipid membrane. Although sesamol can potentially influence the stabilization of zeta potential when encapsulated in SLNs, specific studies and experimental analyses would be needed to confirm this effect and fully understand its mechanism of action.

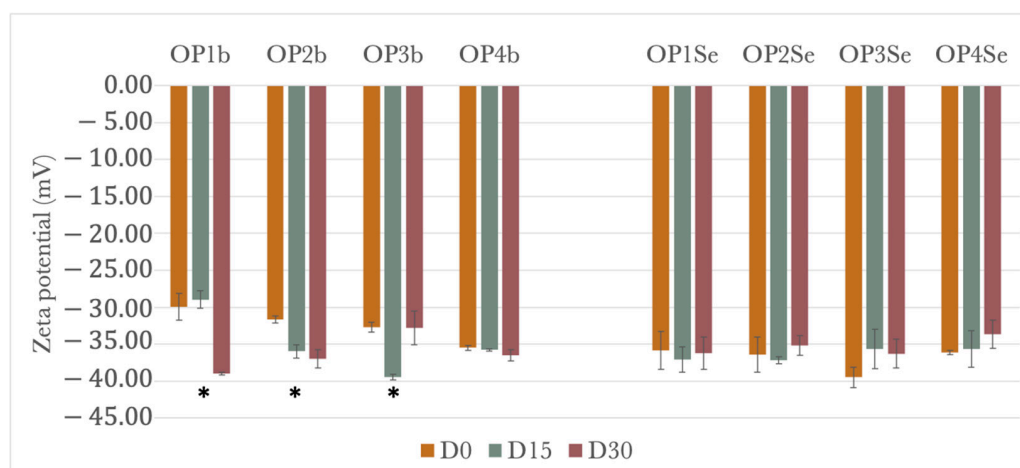


**Figure 5.** Mean zeta potential values of blank and loaded optimized SLNs at different times. \* Significant difference in zeta potential during storage ( $p < 0.05$ ) ( $n = 3$ ).

### 3.6.3. Encapsulation Efficiency Stability

The encapsulation efficiency percentages remained consistently high across all formulations (72–77%) even after a 30-day storage period (Figure 6). The incorporation of sesamol proved to be effective and remained unchanged for OP2Se throughout the storage duration ( $p > 0.05$ ). The worst case, with a release of sesamol close to 1%, was observed for OP3Se.

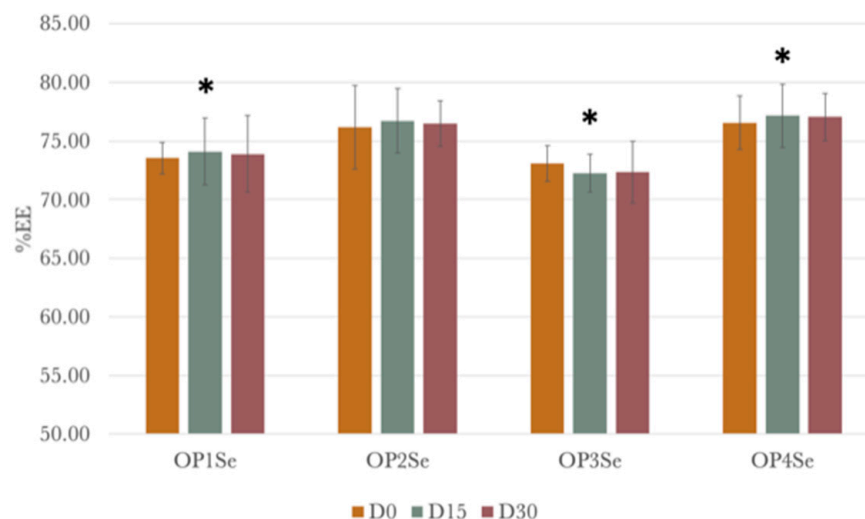


**Figure 6.** Mean encapsulation efficiency percentage values of loaded optimized SLNs at different times. \* Significant difference in encapsulation efficiency percentage during storage ( $p < 0.05$ ).

Carnauba wax is a complex lipid material with different amounts of primarily acid esters, free acids, fatty alcohols, and hydrocarbons. Moreover, carnauba wax contains few free fatty acids (acid value: 2–7) and 5% resins. Due to its composition and chemical properties, carnauba wax probably hardly allows any water to penetrate into the pores of the lipidic structure, which lowers the release of sesamol [28]. Indeed, OP2Se exhibited the smallest variation in the percentage of encapsulation, around 0.39%, with the highest amount of carnauba wax in the SLN core.

#### 3.6.4. Turbiscan Stability

To compare and characterize the physical stability of various formulations, a specific parameter was utilized: the Turbiscan Stability Index (TSI). The principle of this technique is to measure both the transmission and backscattering of infrared light from the bottom to the top of the glass container, which makes it possible to evaluate the stability of the system from the scans. The TSI is a cumulative sum of all the backscattering or transmission variations of the entire sample due to destabilization. Therefore, the higher the TSI is, the more unstable the sample is.

It is important to understand the three stages of TSI: When below 1, no visual destabilization is observed; only very early destabilizations are detected, such as migration or size variation.

Between 1 and 3, the detected variations coincide with the early stages of destabilization but are, for the most part, still not visible. When the TSI is above 3, this is important or extreme destabilization, such as large sedimentation or creaming, wide particle size variation, or phase separation [29].

In our case, the OP3b and OP3Se SLNs (in light blue and dark blue, respectively) were clearly not stable. The TSI value was above 3 after 1 day of analysis and increased with time, especially for the SLNs containing sesamol (Figure 7). Moreover, the percentage of variation of the delta retrodiffusion was around 5% for both formulations, which is also a sign of instability.

The same conclusion can be made for the OP1b and OP1Se SLNs, although the TSIs were between 1 and 3. It is important to note that for the OP1b SLNs, the TSI continued to increase sharply after 1 month of analysis, which is a sign that destabilization was still not over. Indeed, in addition to a high TSI, an increase in the percentage of backscattering can be observed at the top of the glass container around 9% (Figure 8), which could be a sign of creaming even though it was not visible to the naked eye.

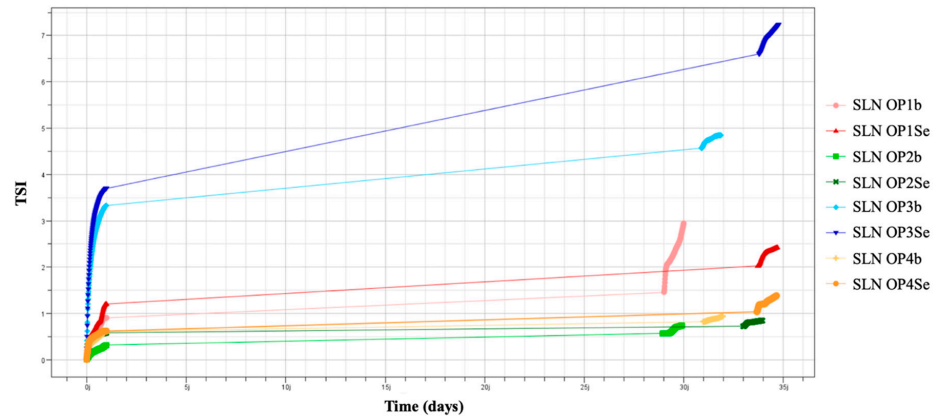


**Figure 7.** Representation of the Turbiscan Stability Index (TSI) of the optimized SLNs with and without sesamol.

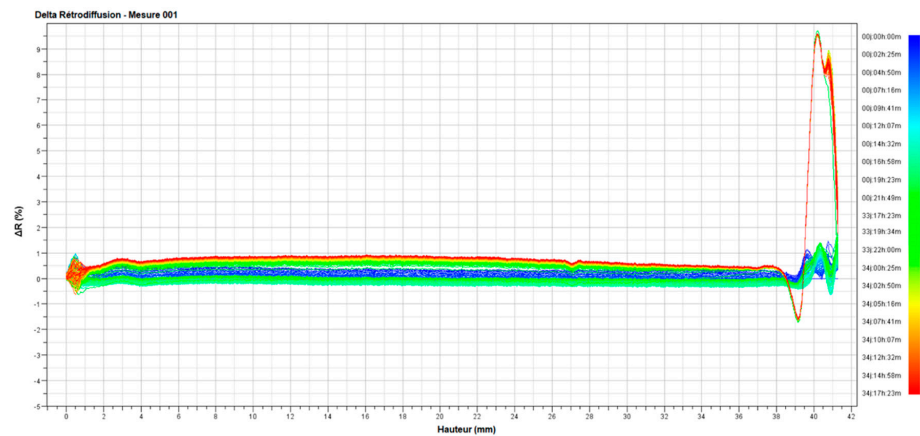


**Figure 8.** Representation of the delta retrodiffusion of OP1Se during storage (example of an unstable formulation).

The OP2 and OP4 SLNs seemed stable with a TSI below or around 1 throughout the duration of the experiment. Moreover, the percentage of variation of backscattering was stable throughout the container (Figure 9). The only difference between the two is that the OP4Se SLNs showed a slight increase in TSI during the last 24 h of analysis, which may be a sign of instability.

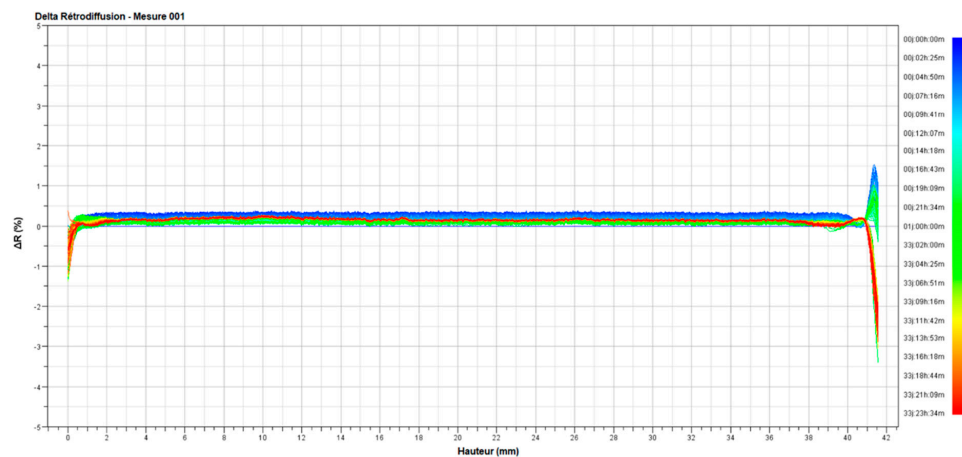


**Figure 9.** Representation of the delta retrodiffusion of OP2Se during storage (example of a stable formulation).



To conclude, at the end of this stability study, we decided to choose the most stable formulation and used it for the microscopy and DSC analyses and the skin penetration study.

If we look at all the stability studies, we can see that the formulations OP1Se and OP3Se showed the poorest results. Indeed, we can see a variation in PS, PDI, and ZP over the storage period for these two formulations. In addition, the TSI graphs do not suggest good stability for these two.

Regarding the TSI, it was more difficult to choose between OP2Se and OP4Se (Figure 7). However, if we look more closely at the stability results, we can see that there was a PS variation for OP4b but not for OP2b, and a slight variation was observed in the %EE for OP4Se. Moreover, we can see that the TSI for OP4Se tended to increase beyond 1.5 over the last 24 h of storage. All these data indicate a poorer stability than OP2Se.

Thus, after careful analysis of all results, the OP2Se formulation was chosen for the electron microscopy, DSC, and skin penetration studies.

### 3.7. Scanning Electron Microscopy (SEM)

To obtain more information on the particle size and morphology, SEM analysis was also performed.

Figures 10 and 11 show images of the OP2b and OP2Se SLNs, respectively. Most of the particles present a spherical shape, but we can see that this is not always the case. Moreover, the sizes of the SLNs observed by SEM ( $250 \pm 50$  nm for OP2b) were shown to be slightly bigger than those obtained by DLS ( $182.77 \pm 6.07$  nm). These phenomena can be explained by the lipid deformation that took place during the drying process of the sample. In addition, the particle shape also depends on the purity of the lipid [3,30]. On the other hand, the SEM confirmed the increase in size between the OP2b and OP2Se SLNs (Figure 10B,C and Figure 11B,C) also observed in DLS (Table 4).

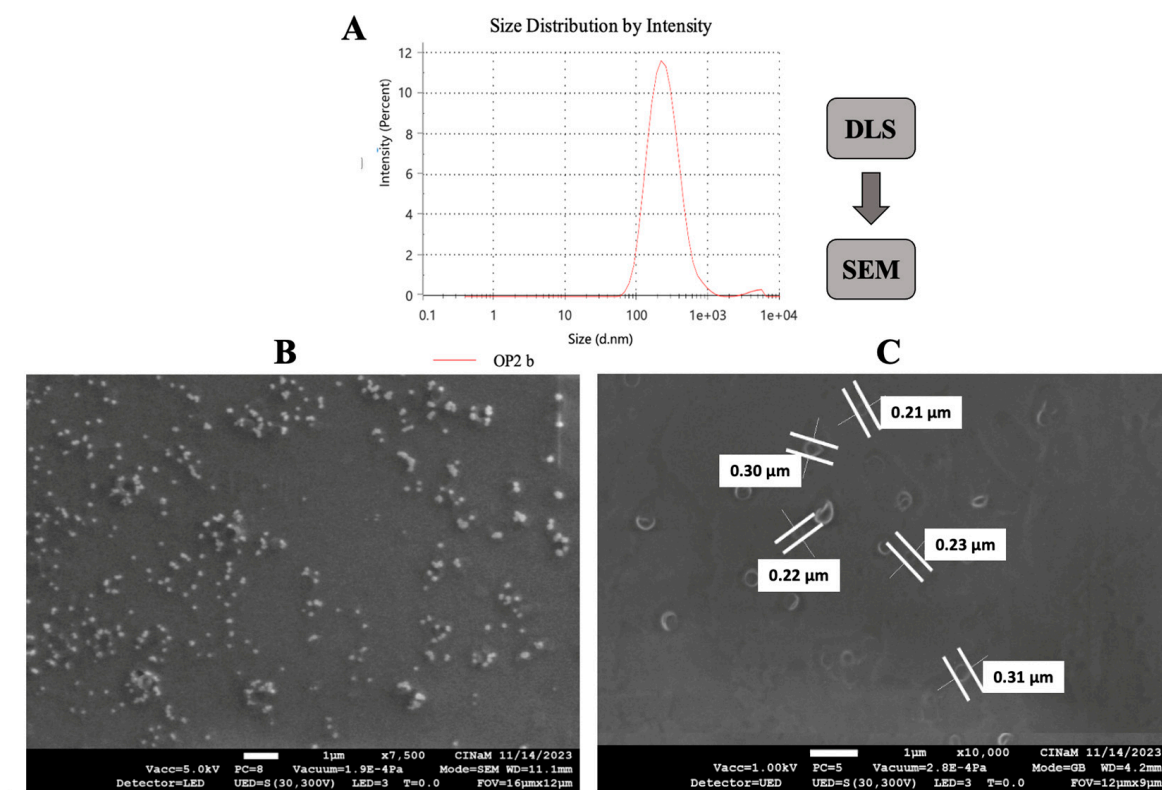


**Figure 10.** Size distribution of OP2b SLNs by DLS measurement (A) and scanning electron microscopy (SEM):  $\times 7500$  (B);  $\times 10,000$  (C).

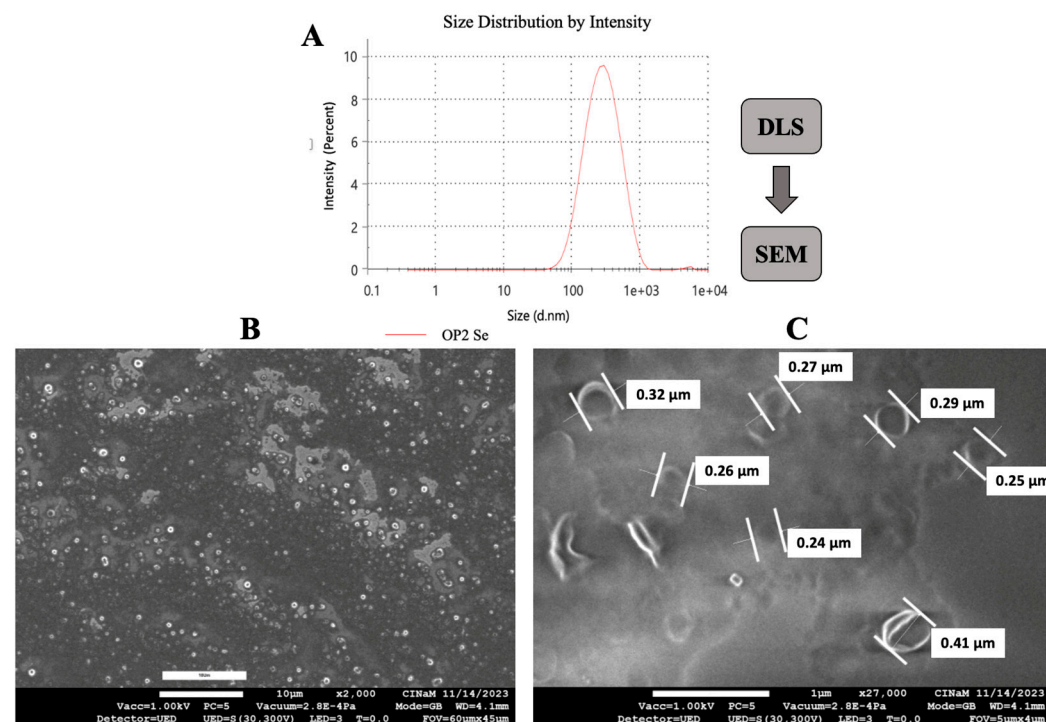


**Figure 11.** Size distribution of OP2Se SLNs by DLS measurement (A) and scanning electron microscopy (SEM):  $\times 2000$  (B);  $\times 15,000$  (C).

### 3.8. Differential Scanning Calorimetry (DSC)

DSC determined the solid-state characterization of OP2 SLNs. DSC was performed for the assessment of the drug–lipid interactions and the crystallinity of sesamol and lipid matrices.

Lipid crystallization is an important point for the performance of SLN carriers. In fact, less perfect crystals with many imperfections can offer space to accommodate the drug [2] and may also modulate the mobility of the drug during the release process. As illustrated in Figure 12, the following samples are analyzed: pure GDS (red), GB (green), CW (blue), and sesamol (brown); in Figure 13, the results for unloaded (blue) and loaded (green) OP2 SLNs can be seen. In Figure 12, a sharp endothermic peak can be observed at around 65–72 °C, which represents the temperature range corresponding to the melting point of sesamol. No such peak was observed in the case of SLNs OP2Se (Figure 13).

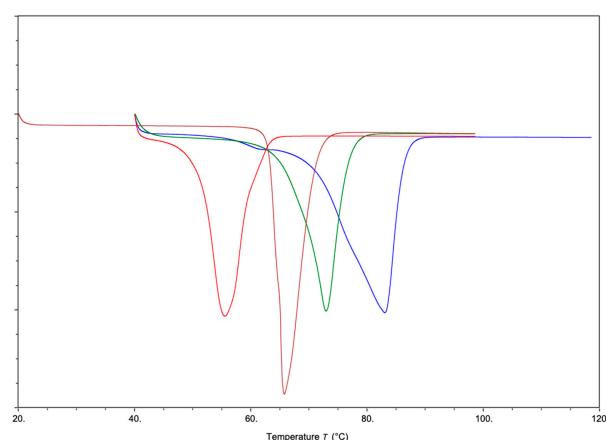


**Figure 12.** DSC thermographs of pure carnauba wax (CW) (blue), glyceryl behenate (GB) (green), glyceryl distearate (GDS) (red), and sesamol (Se) (brown).

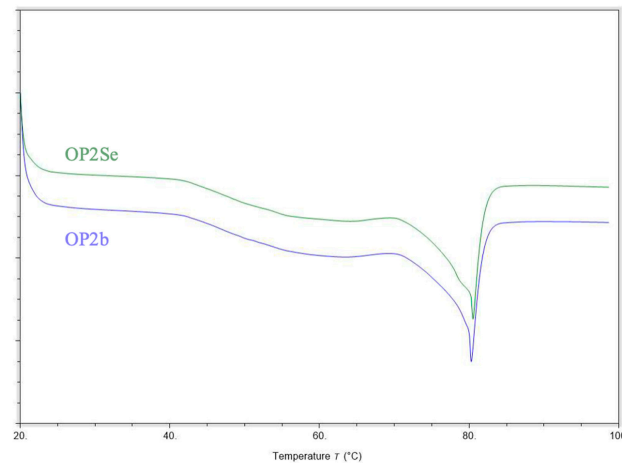


**Figure 13.** DSC thermographs of unloaded (OP2b) and loaded (OP2Se) solid lipid nanoparticles (loaded with 0.2% sesamol and obtained after 10 min of sonication).

The absence of the endothermic peak related to the free drug in the case of OP2Se SLNs substantiated the presumption that the drug was effectively encapsulated within the solid lipid matrix, either in a molecularly dispersed form or in an amorphous state.

### 3.9. *In Vitro* Skin Permeation Studies

*In vitro* release studies and skin permeation studies were performed to compare the release from sesamol-loaded SLNs and solubilized sesamol in hydrogel using Franz diffusion cells. The hydrogel was used as a control to evaluate the skin-targeting ability of sesamol-loaded SLNs. All formulations were prepared with 0.2% sesamol, and the content of sesamol permeated in the skin was analyzed by HPLC. According to the clinical application time, the formulations were applied on the skin surface for a duration of 8 h. The kinetic profile obtained from the hydrogel was compared to the one obtained with OP2Se, which was the most stable optimized SLN formulation (Figure 14).

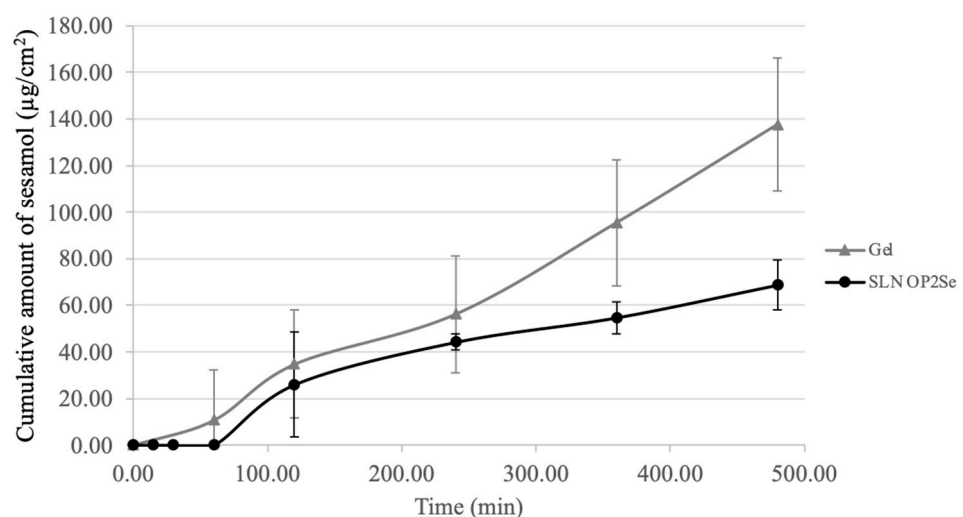


**Figure 14.** Permeation profile of sesamol throughout human skin explant (hydrogel vs. OP2Se SLNs).

Both profiles present the same kinetic release rate of sesamol during the first 4 h. After this period, the release rate from the hydrogel shows a significant increase, whereas the release rate from SLNs stay almost constant.

The amount of sesamol permeated through the skin using the hydrogel and OP2Se SLNs was 137.50 and 68.66 µg/cm<sup>2</sup>, respectively, after 8 h of permeation.

The primary purpose of topically applied cosmetic actives is to provide superficial action or a local effect, as most of these substances are not designed to penetrate the skin deeply or be absorbed into the bloodstream. With time, polymorphic transition and subsequent active ingredient expulsion from SLNs become more likely to occur, reducing the sesamol permeation into deeper skin layers [31]. Indeed, the moderate Log P value suggests that sesamol possesses both lipophilic and hydrophilic characteristics, enabling it to interact with the lipid-rich stratum corneum as well as the aqueous environment of deeper skin layers [32]. Moreover, as mentioned in Table 3, sesamol, with a molecular weight of 138.12 g/mol, is relatively small, which facilitates its permeation through the skin [33]. These factors potentially explain why the penetration of sesamol is more significant in the donor compartment with the hydrogel alone compared to the SLNs. Indeed, the use of lipid nanoparticle dispersions enables us to control the rate at which these actives penetrate the skin [34].

With the use of the SLN system, a significant decrease in sesamol penetration into the receptor compartment could be observed after 8 h of skin penetration. Indeed, Student's *t*-test was applied to the kinetic profiles and a *p*-value < 0.05 was determined. Hence, this system can be useful for cosmetic applications, and careful selection of the SLN wax composition could lead to the desired approach providing active ingredient levels in specific layers of the skin [31].

The results of the permeation studies are reported in Figure 15, which represents the sesamol retention in different parts of the skin and in the receptor fluid of Franz diffusion cells. As can be seen from Figure 15, a higher skin penetration of sesamol can be observed with the hydrogel (with a higher sesamol concentration in the receptor compartment) compared to the SLNs. The SLN system reduces the passage of sesamol through the skin and, by consequence, into the bloodstream. This can be explained in part by the fact that the hydrogel contains some ingredients (such as glycerin and propanediol) which increase skin hydration and promote the penetration of the active by faster diffusion compared to the SLNs (Figure 14) [26].

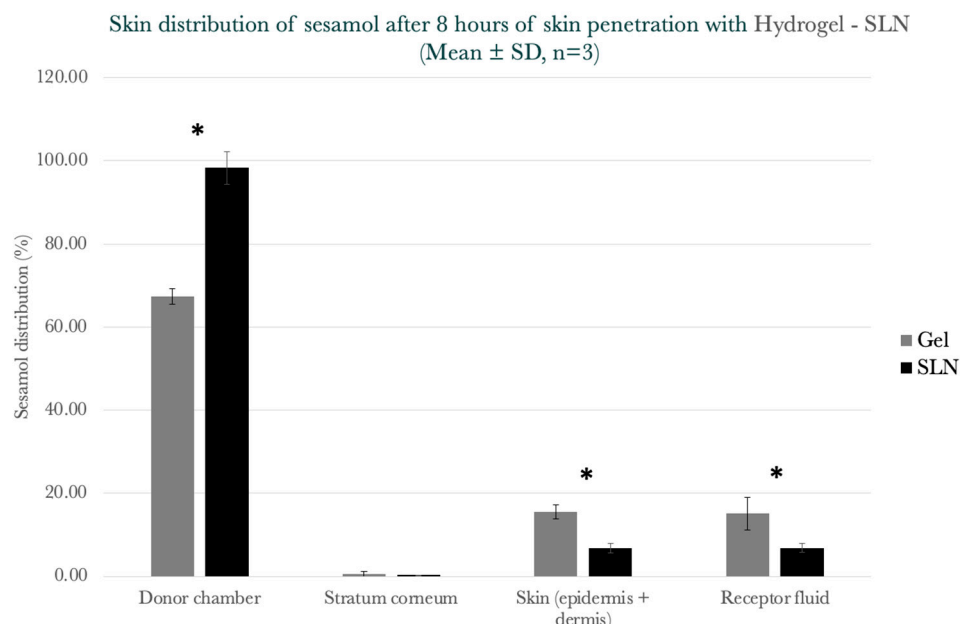


**Figure 15.** Skin distribution of sesamol after 8 h of penetration on human skin explant (hydrogel vs. OP2Se SLNs). \* Significant difference ( $p < 0.05$ ) ( $n = 3$ ).

Moreover, the size of the SLNs has an impact on skin penetration. Since the size of the SLNs was approximately 200 nm, they were probably too big to achieve good penetration into the deeper layer of the skin, and the penetration of the sesamol probably occurred via

a simple slow diffusion. Indeed, the sub-100 nm size range is crucial for the onset of action in dermal drug delivery [4]. However, SLN systems are still an interesting approach.

In fact, this decrease in sesamol penetration is not really a problem. On the contrary, these formulations are destined for cosmetic applications, which means that the most important thing is to reduce bloodstream penetration before increasing skin penetration, which is exactly the case in this study.

To finish, it will be interesting to investigate what happens if we increase the penetration time, for example, to 24 h. Indeed, the amount of sesamol in the receiving compartment tended to stabilize after 8 h of penetration. Moreover, nanoparticles possess a notable characteristic that renders them interesting for topical use: they have a tendency to diffuse and accumulate within hair follicles. These particles can aggregate at the follicular opening and penetrate along the follicular duct when applied to the skin surface [35]. With a 24-h penetration time, the sesamol could reveal better repartition into the skin without a significant increase in bloodstream absorption. Furthermore, it could be interesting to refine the lipidic composition of the SLNs to make them biocompatible in order to promote the intracellular pathway.

Finally, it is also possible to rethink the application of these SLNs for other cosmetic products such as suncare products, which require the presence of SLNs containing mineral filters on the skin surface for optimal skin protection.

#### 4. Conclusions

In conclusion, the present study focused on the potential of sesamol-loaded SLNs as an effective skin delivery system compared to conventional cosmetic vehicles such as our hydrogel.

The results of our stability study revealed that OP2Se was the most suitable in the skin penetration test. Indeed, it presented a stable PS, PDI, ZP, and EE during storage and the TSI value remained below 1 after 1 month, which is a good sign of stability.

The *in vitro* kinetic release and skin permeation studies provided important insights into the behavior of sesamol-loaded SLNs compared to a control hydrogel. The results indicated that the SLNs slowed down the penetration of sesamol through the skin compared to the hydrogel. This controlled release profile is advantageous for cosmetic applications, where localized effects on the skin are desired without significant penetration into the bloodstream. The size of the SLNs, around 200 nm, may have contributed to this controlled release profile.

While the present study has demonstrated the potential benefits of SLNs in controlling the release and penetration of sesamol for cosmetic purposes, further investigations can be carried out to increase sesamol retention in the skin without increasing bloodstream assimilation.

**Author Contributions:** Conceptualization, M.C., C.S. and P.P.; methodology, M.C., A.O., C.O., E.W., L.A., A.A. and M.C.-B.; software, M.C., E.W., L.A., A.A. and M.C.-B.; validation, M.C., L.A., M.C.-B. and C.S.; formal analysis, M.C., A.O. and M.C.-B.; investigation, M.C., A.O., L.A., A.A., M.C.-B. and C.S.; resources, C.O., E.W., L.A., A.A., M.C.-B. and C.S.; data curation, M.C., A.O. and M.C.-B.; writing—original draft preparation, M.C., A.O., M.C.-B. and C.S.; writing—review and editing, M.C., M.C.-B., C.S. and P.P.; visualization, M.C.; supervision, C.S. and P.P.; project administration, C.S. and P.P.; funding acquisition, P.P. All authors have read and agreed to the published version of the manuscript.

**Funding:** This research was funded by Protisvalor (Aix-Marseille Université, France) (funding number: REF PVM 2020-142) and Les Laboratoires Multaler (Yon-Ka Paris) (Argenteuil, France) (funding number: 2019/0294).

**Institutional Review Board Statement:** Not applicable.

**Informed Consent Statement:** Not applicable.



**Data Availability Statement:** The original contributions presented in the study are included in the article, further inquiries can be directed to the corresponding author/s.

**Acknowledgments:** We would like to thank IMCD France (Lyon, France), Gattefossé (Saint-Priest, France), Croda (Montigny-le-bretonneux, France), Cooper (Melun, France), Ies Labo (Oraison, France), AMI ingredient (Tauxigny-Saint-Bauld, France), Evonik (France), and Sigma Aldrich (Saint-Quentin-Fallavier, France) for their contribution to material supplies.

**Conflicts of Interest:** The authors declare no conflicts of interest. The funders had no role in the design of the study; in the collection, analyses, or interpretation of data; in the writing of the manuscript; or in the decision to publish the results.

## References

1. Harivardhan Reddy, L.; Murthy, R.S.R. Etoposide-Loaded Nanoparticles Made from Glyceride Lipids: Formulation, Characterization, in Vitro Drug Release, and Stability Evaluation. *AAPS PharmSciTech* **2005**, *6*, E158–E166. [[CrossRef](#)] [[PubMed](#)]
2. Müller, R.H.; Mäder, K.; Gohla, S. Solid Lipid Nanoparticles (SLN) for Controlled Drug Delivery—A Review of the State of the Art. *Eur. J. Pharm. Biopharm.* **2000**, *50*, 161–177. [[CrossRef](#)] [[PubMed](#)]
3. Teeranachaideekul, V.; Souto, E.B.; Junyaprasert, V.B.; Müller, R.H. Cetyl Palmitate-Based NLC for Topical Delivery of Coenzyme Q(10)—Development, Physicochemical Characterization and in Vitro Release Studies. *Eur. J. Pharm. Biopharm.* **2007**, *67*, 141–148. [[CrossRef](#)] [[PubMed](#)]
4. Mardhiah Adib, Z.; Ghanbarzadeh, S.; Kouhsoltani, M.; Yari Khosroshahi, A.; Hamishehkar, H. The Effect of Particle Size on the Deposition of Solid Lipid Nanoparticles in Different Skin Layers: A Histological Study. *Adv. Pharm. Bull.* **2016**, *6*, 31–36. [[CrossRef](#)] [[PubMed](#)]
5. Silva, A.C.; González-Mira, E.; García, M.L.; Egea, M.A.; Fonseca, J.; Silva, R.; Santos, D.; Souto, E.B.; Ferreira, D. Preparation, Characterization and Biocompatibility Studies on Risperidone-Loaded Solid Lipid Nanoparticles (SLN): High Pressure Homogenization versus Ultrasound. *Colloids Surf. B Biointerfaces* **2011**, *86*, 158–165. [[CrossRef](#)] [[PubMed](#)]
6. Pardeike, J.; Hommoss, A.; Müller, R.H. Lipid Nanoparticles (SLN, NLC) in Cosmetic and Pharmaceutical Dermal Products. *Int. J. Pharm.* **2009**, *366*, 170–184. [[CrossRef](#)]
7. Müller, R.H.; Radtke, M.; Wissing, S.A. Solid Lipid Nanoparticles (SLN) and Nanostructured Lipid Carriers (NLC) in Cosmetic and Dermatological Preparations. *Adv. Drug Deliv. Rev.* **2002**, *54*, S131–S155. [[CrossRef](#)] [[PubMed](#)]
8. Souto, E.B.; Müller, R.H. Cosmetic Features and Applications of Lipid Nanoparticles (SLN, NLC). *Int. J. Cosmet. Sci.* **2008**, *30*, 157–165. [[CrossRef](#)]
9. Mehnert, W.; Mäder, K. Solid Lipid Nanoparticles: Production, Characterization and Applications. *Adv. Drug Deliv. Rev.* **2001**, *47*, 165–196. [[CrossRef](#)]
10. Wissing, S.A.; Müller, R.H. Solid Lipid Nanoparticles as Carrier for Sunscreens: In Vitro Release and in Vivo Skin Penetration. *J. Control. Release* **2002**, *81*, 225–233. [[CrossRef](#)]
11. Cassayre, M. Selection of Natural Active Ingredients Regulating Melanogenesis and Assessment of Skin Penetration, Using a Comparative Approach to Electroporation Techniques and Optimised Nano-Object Formulations. Ph.D. Thesis, Aix-Marseille University, Marseille, France, 2024.
12. Srisayam, M.; Weerapreeyakul, N.; Barusrux, S.; Kanokmedhakul, K. Antioxidant, Antimelanogenic, and Skin-Protective Effect of Sesamol. *J. Cosmet. Sci.* **2014**, *65*, 69–79.
13. Geetha, T.; Rohit, B.; Pal, K.I. Sesamol: An Efficient Antioxidant with Potential Therapeutic Benefits. *Med. Chem.* **2009**, *5*, 367–371. [[CrossRef](#)] [[PubMed](#)]
14. Prado, V.C.; Moenke, K.; Osmari, B.F.; Pegoraro, N.S.; Oliveira, S.M.; Cruz, L. Development of Guar Gum Hydrogel Containing Sesamol-Loaded Nanocapsules Designed for Irritant Contact Dermatitis Treatment Induced by Croton Oil Application. *Pharmaceutics* **2023**, *15*, 285. [[CrossRef](#)] [[PubMed](#)]
15. Wu, P.-Y.; You, Y.-J.; Liu, Y.-J.; Hou, C.-W.; Wu, C.-S.; Wen, K.-C.; Lin, C.-Y.; Chiang, H.-M. Sesamol Inhibited Melanogenesis by Regulating Melanin-Related Signal Transduction in B16F10 Cells. *Int. J. Mol. Sci.* **2018**, *19*, 1108. [[CrossRef](#)] [[PubMed](#)]
16. Mahendra Kumar, C.; Sathisha, U.V.; Dharmesh, S.; Rao, A.G.A.; Singh, S.A. Interaction of Sesamol (3,4-Methylenedioxyphenol) with Tyrosinase and Its Effect on Melanin Synthesis. *Biochimie* **2011**, *93*, 562–569. [[CrossRef](#)] [[PubMed](#)]
17. Madureira, A.R.; Campos, D.A.; Fonte, P.; Nunes, S.; Reis, F.; Gomes, A.M.; Sarmiento, B.; Pintado, M.M. Characterization of Solid Lipid Nanoparticles Produced with Carnauba Wax for Rosmarinic Acid Oral Delivery. *RSC Adv.* **2015**, *5*, 22665–22673. [[CrossRef](#)]
18. Santonocito, D.; Sarpietro, M.G.; Carbone, C.; Panico, A.; Campisi, A.; Siciliano, E.A.; Sposito, G.; Castelli, F.; Puglia, C. Curcumin Containing PEGylated Solid Lipid Nanoparticles for Systemic Administration: A Preliminary Study. *Molecules* **2020**, *25*, 2991. [[CrossRef](#)]
19. Turbiscan LAB: The World Reference Stability Analyzer. Available online: <https://formulaction.com/product/turbiscan-lab/> (accessed on 29 September 2023).
20. Wagner, H.; Kostka, K.-H.; Lehr, C.-M.; Schaefer, U.F. Interrelation of Permeation and Penetration Parameters Obtained from in Vitro Experiments with Human Skin and Skin Equivalents. *J. Control. Release* **2001**, *75*, 283–295. [[CrossRef](#)]



21. Lademann, J.; Jacobi, U.; Surber, C.; Weigmann, H.-J.; Fluhr, J.W. The Tape Stripping Procedure—Evaluation of Some Critical Parameters. *Eur. J. Pharm. Biopharm.* **2009**, *72*, 317–323. [[CrossRef](#)] [[PubMed](#)]
22. Liu, C.-H.; Wu, C.-T. Optimization of Nanostructured Lipid Carriers for Lutein Delivery. *Colloids Surf. A Physicochem. Eng. Asp.* **2010**, *353*, 149–156. [[CrossRef](#)]
23. Das, S.; Chaudhury, A. Recent Advances in Lipid Nanoparticle Formulations with Solid Matrix for Oral Drug Delivery. *AAPS PharmSciTech* **2010**, *12*, 62–76. [[CrossRef](#)]
24. Pinheiro Machado, G.T.; Veleirinho, M.B.; Mazzarino, L.; Machado Filho, L.C.P.; Maraschin, M.; Cerri, R.L.A.; Kuhnen, S. Development of Propolis Nanoparticles for the Treatment of Bovine Mastitis: In Vitro Studies on Antimicrobial and Cytotoxic Activities. *Can. J. Anim. Sci.* **2019**, *99*, 713–723. [[CrossRef](#)]
25. Han, S.B.; Kwon, S.S.; Jeong, Y.M.; Yu, E.R.; Park, S.N. Physical characterization and in vitro skin permeation of solid lipid nanoparticles for transdermal delivery of quercetin. *Int. J. Cosmet. Sci.* **2014**, *36*, 588–597. [[CrossRef](#)]
26. Lai, F.; Sinico, C.; De Logu, A.; Zaru, M.; Müller, R.H.; Fadda, A.M. SLN as a Topical Delivery System for Artemisia Arborescens Essential Oil: In Vitro Antiviral Activity and Skin Permeation Study. *Int. J. Nanomed.* **2007**, *2*, 419–425.
27. Peng, T.-X.; Liang, D.-S.; Guo, F.; Peng, H.; Xu, Y.-C.; Luo, N.-P.; Zhang, X.-Y.; Zhong, H.-J. Enhanced Storage Stability of Solid Lipid Nanoparticles by Surface Modification of Comb-Shaped Amphiphilic Inulin Derivatives. *Colloids Surf. B Biointerfaces* **2019**, *181*, 369–378. [[CrossRef](#)]
28. Özyazıcı, M.; Gökçe, E.H.; Ertan, G. Release and Diffusional Modeling of Metronidazole Lipid Matrices. *Eur. J. Pharm. Biopharm.* **2006**, *63*, 331–339. [[CrossRef](#)]
29. Turbiscan Stability Index (TSI). Available online: <https://formulaction.com/solutions/turbiscan-stability-index-tsi/> (accessed on 29 September 2023).
30. Gomes, M.J.; Martins, S.; Ferreira, D.; Segundo, M.A.; Reis, S. Lipid Nanoparticles for Topical and Transdermal Application for Alopecia Treatment: Development, Physicochemical Characterization, and in Vitro Release and Penetration Studies. *Int. J. Nanomed.* **2014**, *9*, 1231–1242. [[CrossRef](#)]
31. Clares, B.; Calpena, A.C.; Parra, A.; Abrego, G.; Alvarado, H.; Fanguero, J.F.; Souto, E.B. Nanoemulsions (NEs), Liposomes (LPs) and Solid Lipid Nanoparticles (SLNs) for Retinyl Palmitate: Effect on Skin Permeation. *Int. J. Pharm.* **2014**, *473*, 591–598. [[CrossRef](#)]
32. Souto, E.B.; Fanguero, J.F.; Fernandes, A.R.; Cano, A.; Sanchez-Lopez, E.; Garcia, M.L.; Severino, P.; Paganelli, M.O.; Chaud, M.V.; Silva, A.M. Physicochemical and Biopharmaceutical Aspects Influencing Skin Permeation and Role of SLN and NLC for Skin Drug Delivery. *Heliyon* **2022**, *8*, e08938. [[CrossRef](#)]
33. Essendoubi, M.; Gobinet, C.; Reynaud, R.; Angiboust, J.-F.; Manfait, M.; Piot, O. Human Skin Penetration of Hyaluronic Acid of Different Molecular Weights as Probed by Raman Spectroscopy. *Ski. Res. Technol.* **2015**, *22*, 55–62. [[CrossRef](#)]
34. Khezri, K.; Saeedi, M.; Morteza-Semnani, K.; Akbari, J.; Rostamkalaei, S.S. An Emerging Technology in Lipid Research for Targeting Hydrophilic Drugs to the Skin in the Treatment of Hyperpigmentation Disorders: Kojic Acid-Solid Lipid Nanoparticles. *Artif. Cells Nanomed. Biotechnol.* **2020**, *48*, 841–853. [[CrossRef](#)] [[PubMed](#)]
35. Patzelt, A.; Lademann, J. Recent Advances in Follicular Drug Delivery of Nanoparticles. *Expert Opin. Drug Deliv.* **2020**, *17*, 49–60. [[CrossRef](#)] [[PubMed](#)]

**Disclaimer/Publisher’s Note:** The statements, opinions and data contained in all publications are solely those of the individual author(s) and contributor(s) and not of MDPI and/or the editor(s). MDPI and/or the editor(s) disclaim responsibility for any injury to people or property resulting from any ideas, methods, instructions or products referred to in the content.